Mineralogical Magazine (2021), **85**, 879–889
doi:10.1180/mgm.2021.83

CAMBRIDGE UNIVERSITY PRESS

Article

Mineralogy of Ga- and Ge-bearing metallurgical slags from Tsumeb, Namibia

Vojtěch Ettler[1]*, Martin Mihaljevič[1], Ladislav Strnad[2], Radim Jedlicka[3], Bohdan Kříbek[4], Rob J. Bowell[5], Fred Kamona[6] and Ben Mapani[7]

[1] Institute of Geochemistry, Mineralogy and Mineral Resources, Faculty of Science, Charles University, Albertov 6, 128 00 Prague 2, Czech Republic; [2] Laboratories of the Geological Institutes, Faculty of Science, Charles University, Albertov 6, 128 00 Prague 2, Czech Republic; [3] Institute of Petrology and Structural Geology, Faculty of Science, Charles University, Albertov 6, 128 00 Prague 2, Czech Republic; [4] Czech Geological Survey, Geologická 6, 152 00 Prague 5, Czech Republic; [5] SRK Consulting UK Ltd, 17 Churchill Way, Cardiff, CF10 2HH, Wales, United Kingdom; [6] Department of Geology, Faculty of Science, University of Namibia, Private Bag 13301, Windhoek, Namibia; and [7] Department of Mining and Process Engineering, Faculty of Engineering, Namibia University of Science and Technology, Private Bag 13388, Windhoek, Namibia.

Abstract

Gallium (Ga) and germanium (Ge) are technologically important critical elements. Lead blast furnace slags from Tsumeb, Namibia, comprise over two million metric tons of material that contains high levels of Ga (135–156 ppm) and Ge (128–441 ppm) in addition to significant Zn concentrations (up to 11 wt.%) and represent a potential resource for these elements. A combination of mineralogical and chemical methods (PXRD, FEG-SEM-EPMA and LA-ICP-MS) indicated different partitioning of Ga and Ge within the individual slag phases. Gallium is predominantly bound in small euhedral crystals of Zn–Fe–Al spinels (<10 μm in size), exhibiting concentrations in the range of 480–1370 ppm (up to 0.004 atoms per formula unit, apfu). Concentrations of Ga in other phases (e.g. melilite) are systematically below 90 ppm. The principal host of Ge is the silicate glass and, to a lesser extent, silicates (melilite and olivine group phases). Concentrations of Ge in glass attained a concentration of 470 ppm (EPMA), but the LA-ICP-MS analysis of glass matrix containing submicrometre spinel crystallites indicated that average Ge levels vary in the range of 113–394 ppm. In the potential extraction of Ga and Ge, the results indicate that ultrafine milling is needed to liberate the Ga- and Ge-hosting phases prior to metallurgical processing of the slag.

Keywords: slags, Tsumeb, Namibia, gallium, germanium, mineralogy

(Received 11 August 2021; accepted 3 November 2021; Accepted Manuscript published online: 10 November 2021; Associate Editor: Irina O Galuskina)

Introduction

Gallium (Ga) and germanium (Ge) are listed among the most critical elements for industry in the European Union (European Commission, 2020), as well as in other technologically advanced countries (Fortier *et al.*, 2018; Hofstra *et al.*, 2021). Gallium is mostly used to manufacture integrated circuits and optoelectrical devices such as laser diodes, light-emitting diodes (LEDs), photodetectors and solar cells (Moskalyk, 2003; Butcher and Brown, 2014; USGS, 2021a). Germanium also has uses in electronics and solar applications such as fibre/infrared optics or in chemical catalysis (Moskalyk, 2004; Melcher and Buchholz, 2014; USGS, 2021b). Gallium is mostly extracted as a by-product of bauxite processing and, to a much lesser extent, from Zn-processing residues and coal (Butcher and Brown, 2014; Frenzel *et al.*, 2016; USGS, 2021a). In contrast, Ge is mostly associated with Zn or Pb–Zn–Cu sulfide ores and coals (Frenzel *et al.*, 2014; USGS, 2021a,b), and many old deposits and prospects of Zn ores have recently been (re-)examined because of the potential to recover Ge (Saini-Eidukat *et al.*, 2009; Mondillo *et al.*, 2018a,b). In addition, so-called 'metalliferous coals' highly enriched in Ge (grades in the order of hundreds of ppm) located especially in China and Russia are also considered as potential sources of Ge (Melcher and Buchholz, 2014 and references therein).

During the pyrometallurgical processing of sulfide ores, Ga and Ge mostly end up in the slag phase due to a strong affinity with Al (Ga) and Si (Ge) (Piatak and Ettler, 2021). Recent laboratory experiments simulating Cu pyrometallurgy confirmed that Ga was partitioned predominantly into the slag phase, but Ge, present in significantly lower concentrations, was almost entirely vaporised (Avarmaa *et al.*, 2019). However, under reducing Pb smelting conditions, Ge was incorporated into silicate slag, with minor volatilisation and only a limited amount dissolved into the Pb metal (Yan and Swinbourne, 2003). Old slag deposits have also been reported as a potential source of Ga and Ge.

*Author for correspondence: Vojtěch Ettler, Email: ettler@natur.cuni.cz
Cite this article: Ettler V., Mihaljevič M., Strnad L., Jedlicka R., Kříbek B., Bowell R.J., Kamona F. and Mapani B. (2021) Mineralogy of Ga- and Ge-bearing metallurgical slags from Tsumeb, Namibia. *Mineralogical Magazine* **85**, 879–889. https://doi.org/10.1180/mgm.2021.83

© The Author(s), 2021. Published by Cambridge University Press on behalf of The Mineralogical Society of Great Britain and Ireland. This is an Open Access article, distributed under the terms of the Creative Commons Attribution-NonCommercial-NoDerivatives licence (http://creativecommons.org/licenses/by-nc-nd/4.0), which permits non-commercial re-use, distribution, and reproduction in any medium, provided that no alterations are made and the original article is properly cited. The written permission of Cambridge University Press must be obtained prior to any commercial use and/or adaptation of the article.

Downloaded from http://pubs.geoscienceworld.org/minmag/article-pdf/85/6/879/5512245/s0026461x21000839a.pdf
by guest

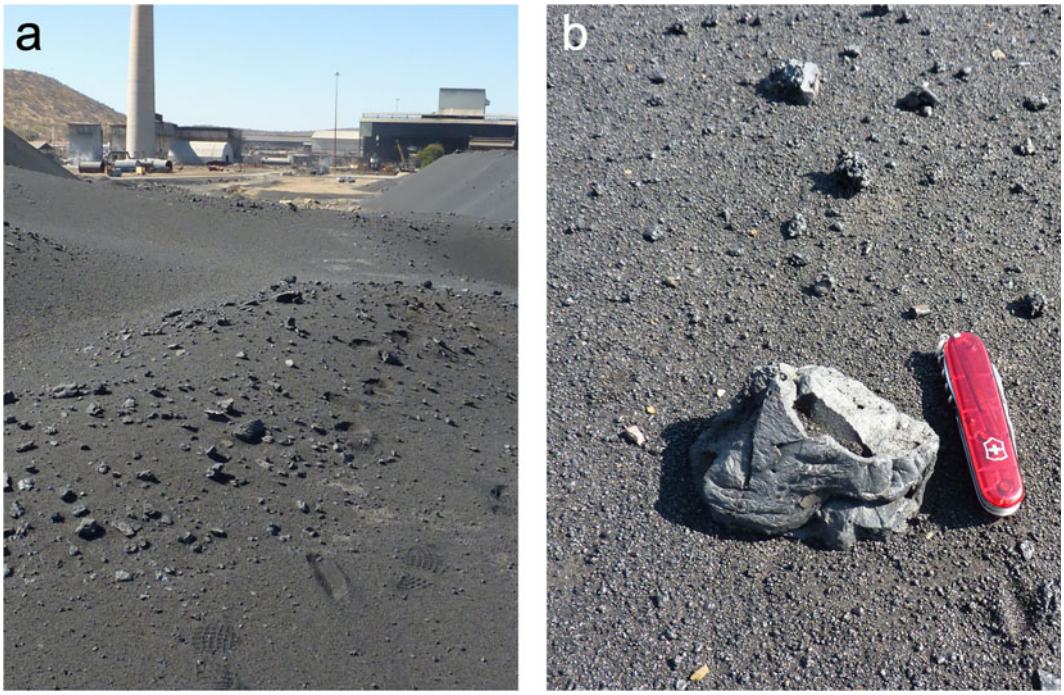

Fig. 1. Field photographs of Ga- and Ge-bearing slags from Tsumeb, Namibia, taken in 2012. (a) View from the top of the dump; (b) massive fragment of slag on the surface of granulated slag dump.

As an example, the 15 Mt slag heap in Lubumbashi, Democratic Republic of Congo produced by processing Kipushi Ge-rich Zn–Cu ores and stratiform Cu–Co ores contains Ge concentrations ranging from 100 to 250 ppm, and is potentially the largest known occurrence of Ge (Melcher and Buchholz, 2012).

Other interesting sites occur in Otavi Mountain Land in northern Namibia, where some Ge-rich sulfide deposits (e.g. Tsumeb and Khusib Springs) have been discovered with ore grades up to 0.83% Ge found predominantly in sulfides (Melcher, 2003; Melcher *et al.*, 2006; Höll *et al.*, 2007; Kamona and Günzel, 2007). These Ga- and Ge-bearing polymetallic sulfide ores mined in the area were historically processed in the Tsumeb smelter, and old slag deposits are now reported as a potential source of Ge (and Ga) (Höll *et al.*, 2007; Frenzel *et al.*, 2014).

Our previous investigations of the Tsumeb metallurgical slags of various ages and produced from different technologies, reported typical concentrations of Ga and Ge in the order of tens ppm (up to 48 ppm Ga, 123 ppm Ge; Ettler *et al.*, 2009a; Jarošíková *et al.*, 2017). Another screening study has shown recently that some old Cu slags from Tsumeb can contain ~100 ppm Ga (Lohmeier *et al.*, 2021). Recovery of Ga and Ge from waste materials and intermediate products is mostly carried out via hydrometallurgical processing (Fayram and Anderson, 2008; Liu *et al.*, 2016; Drzazga *et al.*, 2018) or chloride fuming processes (Dey *et al.*, 2010). However, the design of the metallurgical technology should be based on a detailed knowledge of solid-phase partitioning of target elements within the material. Chirkst *et al.* (2008) proposed a complex chloride leaching and a sorption-based hydrometallurgical method for Zn and Ge recovery from Ga- and Ge-rich slags from Tsumeb. The challenge with the proposed technology was the poor understanding of contaminant elements within the slag and incorporation of these into the products that compromised the quality of the metal oxides produced. In addition, the sensitive nature of the proposed D-403 anionic ion exchange resin made the project uneconomic as a metal process at the time of evaluation. To improve the opportunity to recover these metals from the slag it is essential that the material is characterised in terms of mineralogy and distribution of Ga and Ge in the individual phases. This work aims to characterise the speciation and mineralogy of Ga and Ge within the Tsumeb lead blast-furnace slag materials through a combination of mineralogical and chemical methods such as powder X-ray diffraction (PXRD), scanning electron microscopy and electron microprobe with field emission gun electron source (FEG-SEM-EPMA), and laser ablation inductively coupled plasma mass spectrometry (LA-ICP-MS).

Experimental methods

Sample collection and processing

Slags were collected (with the assistance of smelter staff) in the Tsumeb smelter area during a field campaign in 2012 (GPS coordinates: −19.2255, 17.7226) from the historic reduced Pb blast-furnace slag, produced up to 1996. The smelter was officially commissioned in 1963 by Tsumeb Corporation Limited (TCL). At the time of working, the smelter consisted of a Pb section (including a refinery), a Cu section, and plants that produced Cd, Na antimonite and As_2O_3. Production commenced in early 1964, with 3500 tonnes of Cu and 6000 tonnes of Pb being produced per month. The slag originated from the second stage of the reverberatory furnaces that produced Pb from Cu-depleted feed material. This part of the smelter is currently being dismantled (Dundee Precious Metals, personal communication, 2021).

The dumps were composed mainly of granulated slags, but massive slag fragments were also encountered (Fig. 1). Samples denoted as T17 corresponded to 'Ge slags' (aged ~30 years at the time of sampling), and samples denoted as T18 corresponded to 'Zn slags' (aged ~20 years at the time of sampling) (H. Nolte

Downloaded from http://pubs.geoscienceworld.org/minmag/article-pdf/85/6/879/5512245/s0026461x21000839a.pdf
by guest

and M. Trust, personal communication, 2012). Five samples were collected: three massive slag specimens grabbed on the dump surfaces and two representative granulated slags collected as composite samples from several randomly selected sites of the dump. Höll *et al.* (2007) estimated that the two dumps of Ga- and Ge-rich slags account for 2.9 Mt of material grading 9% Zn, 2.05% Pb, 183 ppm Ge, 200 ppm Ga, and could yield ~800 t Ge, thus representing a major Ge source. Today we know that only 2.2 Mt of these slags remain at the dumps, because some of it was used to cover the nearby tailing pile to reduce the air dispersion of tailing-derived dust particles.

For the microscopic observations, SEM, EPMA and LA-ICP-MS analyses, aliquot parts of the samples were embedded in an epoxy resin and prepared as polished (thin) sections. Other sample aliquots were pulverised in an agate planetary mill (Retsch PM 400, Germany) and used for bulk chemistry and phase-composition determinations.

Bulk chemistry

Determination of major-element composition of the slags was carried out via standard silicate analysis used for rock materials (combination of gravimetric, volumetric, and spectrometric analyses) as described in Ettler *et al.* (2009a). The contents of total sulphur (S_{tot}) and total organic carbon (C_{org}) were determined using a combination of ELTRA CS 530 and ELTRA CS 500 TIC analysers (ELTRA, Germany). For the determination of trace elements in slags, we used two digestion procedures (modified from Strnad *et al.*, 2005) because when preparing samples for the Ge analysis, the usage of $HClO_4$ or HCl during the digestion procedures may lead to Ge loss due to the formation of volatile $GeCl_4$ (Biver and Filella, 2018). The following procedure was used for all the elements studied except Ge: a mass of 0.2 g of sample was dissolved in a closed system (Teflon beakers, Savillex, USA) in a mixture of 10 ml of HF (49% v/v) and 0.5 ml $HClO_4$ (70% v/v) on a hot plate (130°C). The mixture was evaporated to dryness, and this procedure was repeated with 5 ml of HF and 0.5 ml of $HClO_4$. The residue was then evaporated to near dryness, dissolved in 2% HNO_3 (v/v), and diluted to 100 ml before the analysis. A modified digestion procedure was used for the analysis of Ge and avoided the use of chlorate: a mass of 0.2 g of sample was dissolved in a closed system (Teflon beakers, Savillex, USA) in a mixture of 10 ml of HF (49% v/v) and 0.5 ml HNO_3 (65% v/v) on a hot plate (130°C). The mixture was evaporated to dryness, and this procedure was repeated with 5 ml of HF and 0.5 ml of HNO_3. The residue was then evaporated to near dryness, dissolved in 2% HNO_3 (v/v) and diluted to 100 ml before the analysis. All chemicals were reagent-grade (Sigma-Aldrich, Germany), and deionised water obtained by a Millipore Academic (Millipore, USA) system was used for the dilutions.

The digests were analysed for a series of metals and metalloids using a combination of inductively coupled plasma optical emission spectrometry (ICP-OES, Agilent 5110, USA; As, Ba, Cu, Mo and Zn) and quadrupole-based inductively coupled plasma mass spectrometry (ICP-MS, ThermoScientific, iCAP-Q^{TM}, Germany; Ag, Bi, Cd, Co, Cr, Cu, Ga, Ge, In, Ni, Pb, Sb, Se, Sn and V). The ^{71}Ga and ^{74}Ge isotopes were used during the ICP-MS analysis, while the isotopes of other elements were selected as recommended by the manufacturer.

Quality control/quality assurance (QC/QA) of the bulk-digestion procedures and analyses was checked by parallel processing of several certified reference materials: NIST 1633 (Coal Fly Ash), NIST 2782 (Industrial Sludge), NIST 2780 (Hard Rock Mine Waste), BCR-2 (Basalt, British Columbia, USGS), AGV-2 (Andesite, Guano Valley, USGS). The results were found to be satisfactory (Supplementary Table S1).

Mineralogical investigations

Phase compositions of the slags were determined by powder X-ray diffraction analysis (PXRD) using a PANalytical X'Pert Pro diffractometer with Bragg-Brentano geometry (PANalytical, the Netherlands) and an X'Celerator detector (conditions: Cu*K*α radiation, 40 kV, 30 mA, 2 theta range of 5–70°, a step size of 0.02° and counting time 150 s per step). The diffraction patterns obtained were analysed by the *X'Pert High Score Plus 3.0* software coupled with the Crystallography Open Database (COD) (Gražulis *et al.*, 2012).

Polished (thin) sections of the specimens were first examined under a Leica DM LP polarising microscope (Leica, Germany). A JEOL JXA–8530F (JEOL, Japan) electron probe microanalyser (EPMA) equipped with a field emission gun source (FEG), energy dispersion spectrometer (EDS; JEOL JED–2300F), and five wave-dispersion spectrometers (WDS) was used for scanning electron microscopic (SEM) imaging, EDS analyses and quantitative analyses.

The lowest detection limits for our EPMA measurements of oxides and silicates (accelerating voltage of 15 kV and beam current of 20 nA) were 70 ppm for Ga and 90 ppm for Ge. For analyses of sulfides and metallic phases the EPMA was run at 20 kV and 30 nA, and the detection limits were slightly lower (Ga: 40 ppm and Ge: 60 ppm), however none of these elements were detected in any of these phases (see also results below). The standards for measurements were GaAs for Ga (*L*α) and Rb-glass containing 54.09 ± 0.07 wt.% GeO_2 for Ge (*L*α) or germanium metal (*K*α). Detailed analytical conditions and standards used for the instrument calibration are given in Supplementary Table S2.

Laser ablation ICP-MS

Laser ablation ICP-MS was carried out mainly on granulated slag samples (prepared as polished sections) because the textures in massive slags were too fine and complex (with crystals often <10 μm in size) such that it was almost impossible to find areas suitable for the analysis. The LA-ICP-MS was carried out on a NewWave Nd:YAG laser with an output wavelength of 213 nm coupled to a ThermoScientific iCAP-Q^{TM} ICP-MS. Ablated spots were 40–80 μm in diameter, fired with laser energy of 350 μJ at a repetition frequency of 10 Hz; total ablation time was 100 s. Aluminium (^{27}Al) was employed as an internal standard, based on EPMA measurements of Al_2O_3 content in the studied phases. The data were processed externally in a MS Excel spreadsheet-based program, and ^{71}Ga and ^{74}Ge isotopes were used for the concentration determinations. BCR-2G certified reference material was used as an external calibrator of the LA-ICP-MS measurements. The measured values (Ga: 21 ± 1 ppm and Ge: 1.4 ± 0.1 ppm, $N = 11$) were in an excellent agreement with the certified (Ga: 23 ± 1 ppm) or reported values (Ge: 1.5 ± 0.1 ppm), as published in the GeoREM database as 'preferred values' (http://georem.mpch-mainz.gwdg.de). For detailed analytical protocol and correction strategy see Strnad *et al.* (2005, 2009).

Results

Bulk chemistry

The slags studied are typically Si–Ca–Fe rich materials with relatively high concentrations of trace elements (in ppm): Zn

Downloaded from http://pubs.geoscienceworld.org/minmag/article-pdf/85/6/879/5512245/s0026461x21000839a.pdf
by guest

Table 1. Bulk chemical compositions of Ga- and Ge-bearing slags from Tsumeb, Namibia (mean ± standard deviation for trace elements, $N = 2$).*

Sample no.	T17-1A	T17-1B	T18-1	T17-2	T18-2
Sample type	massive	massive	massive	granulated	granulated
wt.%					
SiO_2	35.68	33.32	28.84	35.41	30.27
TiO_2	0.20	0.20	0.16	0.18	0.18
Al_2O_3	4.60	4.66	3.60	4.13	3.81
Fe_2O_3	3.40	8.02	7.24	5.70	7.32
FeO	18.80	13.71	17.20	16.03	15.14
MnO	0.34	0.33	0.23	0.31	0.26
MgO	4.81	5.18	4.83	4.75	5.09
CaO	20.82	20.16	21.72	19.53	19.92
Na_2O	0.55	0.54	0.45	0.62	0.66
K_2O	0.46	0.46	0.43	0.49	0.48
P_2O_5	0.23	0.22	0.38	0.19	0.28
S_{tot}	0.60	0.68	0.46	0.61	0.47
C_{org}	0.04	0.22	0.06	0.15	0.07
LOI	−0.17	0.28	.13	0.06	0.06
ppm					
Ag	67 ± 25	43 ± 7	116 ± 44	84 ± 53	57 ± 33
As	3650 ± 26	1700 ± 6	2880 ± 289	2550 ± 11	3170 ± 107
Ba	2560 ± 6	2640 ± 20	2260 ± 23	999 ± 0.3	1750 ± 13
Bi	1.5 ± 0.26	1 ± 0.1	12 ± 1.2	1 ± 0.2	12 ± 2.8
Cd	139 ± 0.05	56 ± 0.5	116 ± 23	21 ± 0.4	36 ± 2.8
Co	90 ± 1.2	97 ± 0.2	109 ± 3	123 ± 1.4	132 ± 7
Cr	179 ± 0.5	197 ± 5	172 ± 3	331 ± 6	411 ± 39
Cu	3170 ± 14	2530 ± 26	4080 ± 114	3770 ± 30	3750 ± 112
Ga	135 ± 0.8	142 ± 0.7	152 ± 10	144 ± 1.3	156 ± 9
Ge	144 ± 0.7	128 ± 0.2	214 ± 3	285 ± 1.2	441 ± 2
In	3.3 ± 0.03	3 ± 0.01	4.8 ± 0.4	2 ± 0.01	2.6 ± 0.03
Mo	2380 ± 5	2560 ± 28	2570 ± 137	2280 ± 19	2470 ± 154
Ni	9.0 ± 0.5	8 ± 1.3	10 ± 0.4	12 ± 0.3	13 ± 0.7
Pb	20,900 ± 32	14,500 ± 309	21,300 ± 2000	23,000 ± 386	24,800 ± 814
Sb	73 ± 0.7	48 ± 0.02	90 ± 10	75 ± 0.8	125 ± 5
Se	26 ± 0.02	16 ± 0.4	30 ± 2.4	10 ± 0.2	23 ± 1.7
Sn	160 ± 1.3	130 ± 1.5	188 ± 9	89 ± 1.6	115 ± 2
V	161 ± 6	160 ± 1.5	188 ± 29	138 ± 2	130 ± 11
Zn	98,900 ± 653	84,700 ± 1140	106,000 ± 2010	90,600 ± 1270	110,000 ± 1970
Total	103.64	98.98	99.78	100.62	98.78

*S_{tot} – total sulphur; C_{org} – organic carbon; LOI – loss on ignition; Total = sum of oxides + S_{tot} + C_{org} + LOI + metal(loid)s in elemental form.

(84,700–110,000), Pb (14,500–24,800), Cu (2530–4080), Mo (2280–2570), As (1700–3650) and Ba (999–2640). The concentrations of Ga and Ge vary in the range of 135–156 ppm and 128–441 ppm, respectively (Table 1). Compared to our previous analyses of other Tsumeb slags (scatter plot in Fig. 2; Ettler *et al.*, 2009a; Jarošíková *et al.*, 2017), the concentrations of Ga and Ge in the slags studied are substantially higher and correspond well to bulk chemistry data for these Ga- and Ge-rich slags reported elsewhere (Höll *et al.*, 2007; Chirkst *et al.*, 2008).

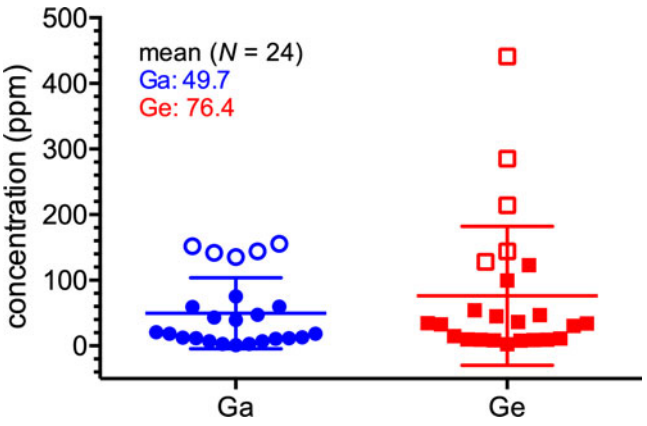

Fig. 2. Scatter plot showing the variability of Ga and Ge concentrations in the Tsumeb slags. Data taken from Ettler *et al.* (2009a), Jarošíková *et al.* (2017), and unpublished results (Ga- and Ge-rich samples investigated in this study are indicated with empty symbols).

Slag petrography

Representative slag textures and phase assemblages for massive and granulated slags are reported in Figs 3 and 4, respectively. Even though anthropogenic materials do not fulfil the criteria for being minerals, in this paper we use mineral names for their synthetic equivalents for the sake of clarity in defining solid phase compositions.

In the massive slags, spinel is the first crystallising phase, followed by melilite, which often contains wüstite exsolutions (Fig. 3b,d,e). The crystallisation sequence continues with the formation of olivine-group phases and residual glass (Fig. 3b,d), which may also contain small wüstite dendrites (Fig. 3f). The silicate matrix contains numerous droplets of metallic/sulfide phases: (1) larger inclusions (<100 μm in size) of complex composition and (2) small droplets (often less than several μm in size), embedded in the glass and other phases, and composed mostly of metallic Pb or galena (PbS) (Fig. 1a,b,d,f). The large inclusions are commonly composed of various sulfides (chalcocite, Cu_2S, and

Downloaded from http://pubs.geoscienceworld.org/minmag/article-pdf/85/6/879/5512245/s0026461x21000839a.pdf
by guest

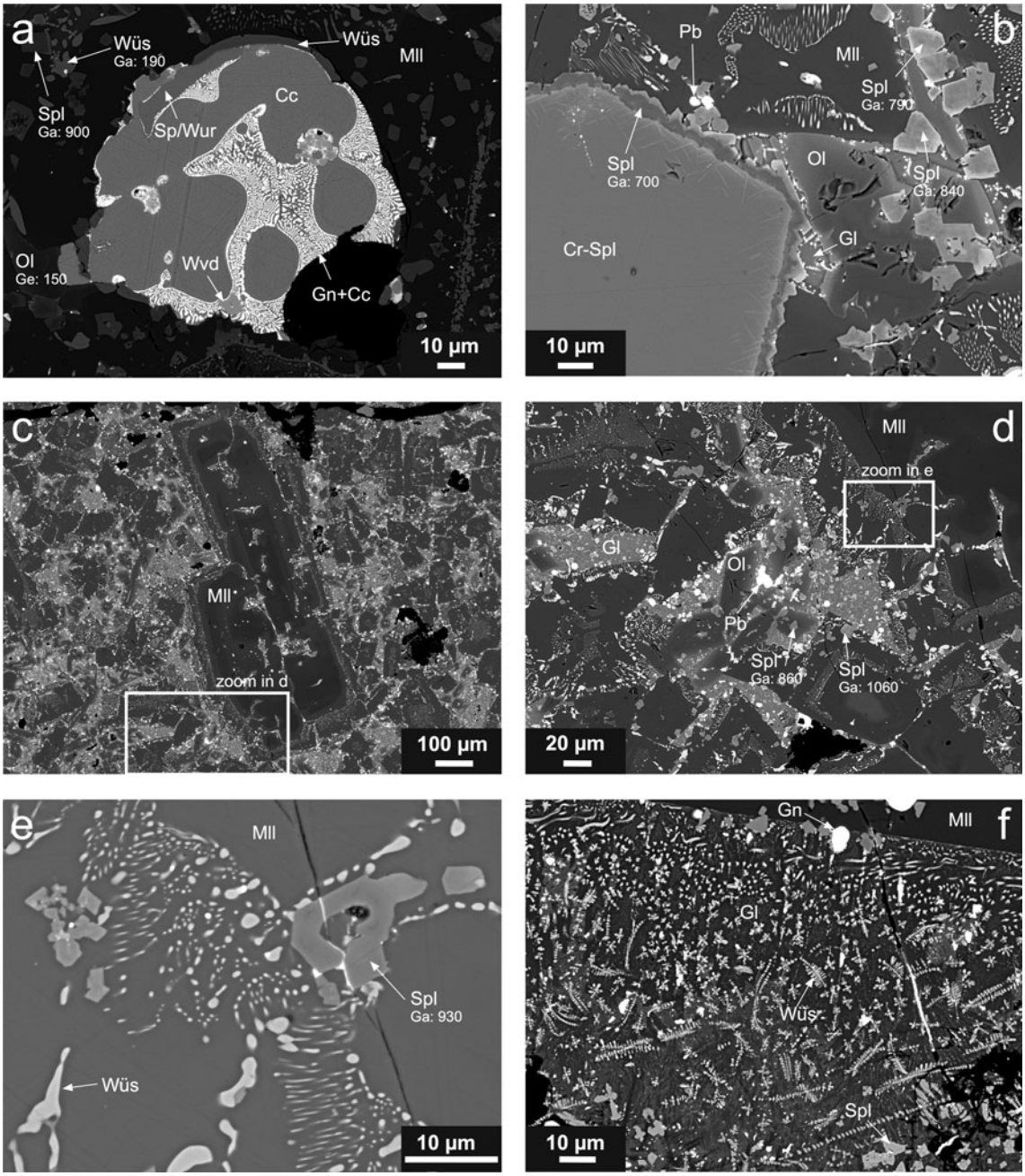

Fig. 3. Scanning electron micrographs of massive slag samples. (a) Sulfide droplet composed of chalcocite (Cc) and chalcocite–galena (Gn) myrmekite, with included crystals of sphalerite/wurtzite (Sp/Wur) and westerveldite (Wvd). The droplet is embedded in a silicate matrix composed of olivine (Ol) and melilite (Mll) with the wüstite (Wüs) and spinel (Spl) dendrites (sample T17-1A). (b) Large Cr-bearing spinel (Cr-Spl) crystal with a Ga-containing spinel rim and euhedral spinel crystals in a silicate matrix composed of melilite, olivine and glass containing Pb droplets (sample T17-1A). (c and d) Large melilite crystals associated with a silicate matrix composed of olivine and glass with euhedral spinel crystals and Pb inclusions (sample T17-1B). (e) Ga-bearing spinel crystals and wüstite exsolutions in melilite. (f) Euhedral spinel crystals, galena droplets and wüstite dendrites within a glass associated with a large melilite crystal (sample T18-1). Phase abbreviations according to Warr (2021). Gallium and germanium concentrations (in ppm) in individual phases are indicated.

chalcocite–galena symplectite, sphalerite/wurtzite, ZnS, and intermetallic phases such as westerveldite, FeAs) (Fig. 1*a*).

Granulated slags exhibit much simpler phase compositions and textures, indicating quenching of the slag melt. Glass is a dominant phase in the samples, and it often contains submicrometre crystals of spinel-group phases and inclusions of metallic Pb (Fig. 4). Spinels are quite common: they either form tiny euhedral crystals embedded in glass or melilite (<10 µm in size) (Fig. 4*a*) or larger blebs (up to ~100 µm in size) (Fig. 4b–d). Large Cr-bearing spinel crystals are relatively rare (Fig. 4c). Melilite forms skeletal crystals indicating rapid cooling of the melt (Fig. 4a).

Crystal chemistry and Ga and Ge partitioning in individual phases

Despite our expectations that Ga and Ge may be bound in sulfides (e.g. sphalerite; Johan, 1988; Saini-Eidukat *et al.*, 2009; Frenzel

Downloaded from http://pubs.geoscienceworld.org/minmag/article-pdf/85/6/879/5512245/s0026461x21000839a.pdf
by guest

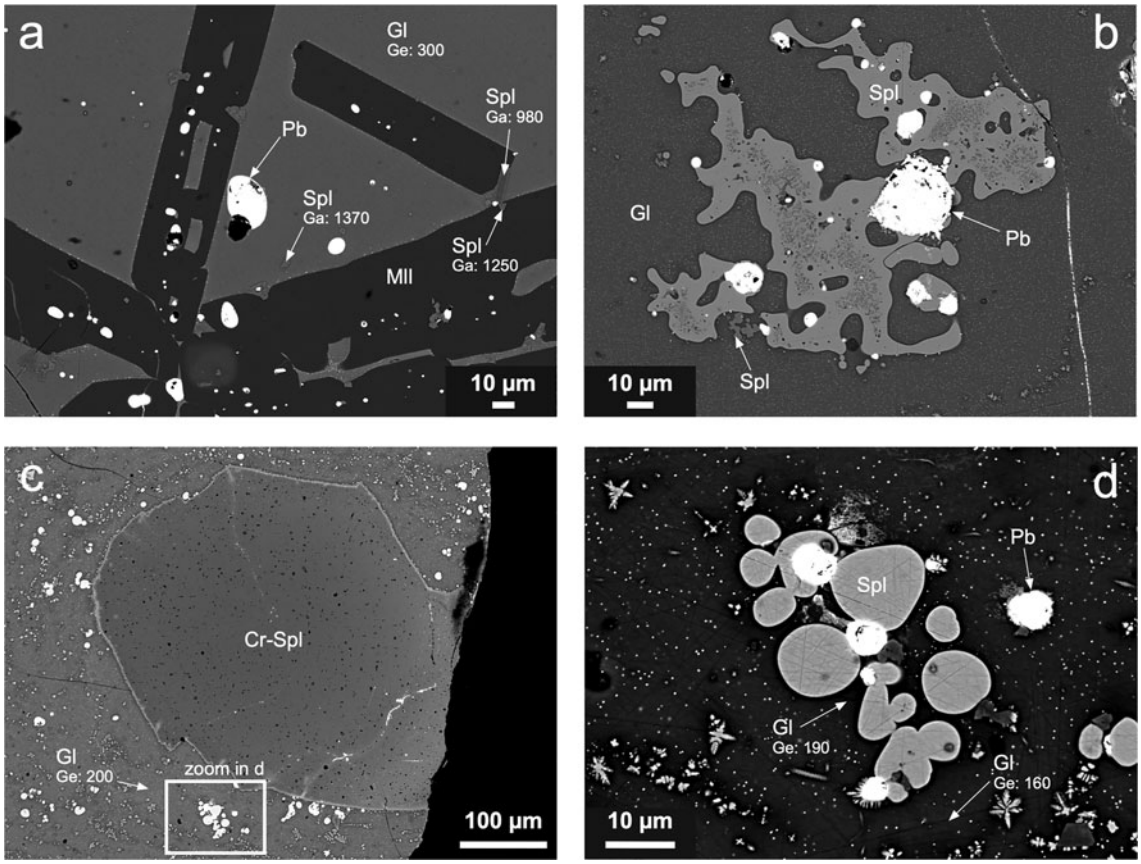

Fig. 4. Scanning electron micrographs of granulated slag samples. (a) Large melilite (Mll) crystals, Pb droplets, and euhedral spinels (Spl) within a glassy matrix (Gl) (sample T17-2). (b) Spinel blebs associated with Pb droplets embedded in glass containing submicrometric spinel crystals and metallic droplets (sample T18-2). (c) Large Cr-bearing spinel embedded in glass (sample T18-2). (d) Oval blebs of spinel and Pb droplets embedded in Ge-bearing glass (sample T18-2). Phase abbreviations according to Warr (2021). Gallium and germanium concentrations (in ppm) in individual phases are indicated.

et al., 2016; Mondillo *et al.*, 2018a), our EPMA data indicated that the slag sulfides contain no Ga or Ge in concentrations above the detection limit of the method. In addition, the small size of the sulfide and metallic inclusions precluded trace-element analysis by LA-ICP-MS. The EPMA results for individual silicate and oxides phases are given in Tables 2–4, and the LA-ICP-MS data are reported in Table 5.

The EPMA showed that the oxyspinels are the key hosts of Ga in the slag. However, large variability in their compositions has been found (Table 2). The Zn–Fe–Al spinels, which according to classification (Bosi *et al.*, 2019) correspond to gahnite, ($ZnAl_2O_4$), hercynite ($FeAl_2O_4$) and magnetite ($Fe^{2+}Fe^{3+}_2O_4$) and form small euhedral crystals and rims (Fig. 3a,b,d,e), are Ga-rich and contain between 480 and 1370 ppm Ga. The most Ga-rich spinel was identified as gahnite with a chemical formula corresponding to $(Zn_{0.453}Mg_{0.336}Fe^{2+}_{0.232}Al_{1.214}Cr_{0.404}Fe^{3+}_{0.297})O_4$, and Ga content in this spinel accounted for 0.004 apfu. In contrast, Cr-bearing spinels forming larger crystals (Figs 3b and 4c) exhibit low Ga concentrations (zincochromite, $ZnCr_2O_4$, analysis 52 in Table 2, 170 ppm Ga) or are Ga-free (magnesiochromite, $MgCr_2O_4$, analyses 23 and 68 in Table 2). The LA-ICP-MS analyses of the large Cr-bearing spinel crystals indicate mean concentrations of 36 ppm Ga and 5 ppm Ge and the magnetite-dominant spinels within the glass exhibit on average 33–99 ppm Ga and 23–73 ppm Ge (the latter element probably being related to a Ge-bearing glass phase in the sample analysed in a mixture with the spinel) (Table 5).

In addition, we also detected Ga via EPMA in some wüstite dendrites (up to 190 ppm Ga [analyses not shown]; Fig. 3a) and rarely in melilite (90 ppm Ga; analysis 60 in Table 3) in the crystalline slags. The LA-ICP-MS analyses indicated that the melilites in granulated slags exhibit 51–74 ppm Ga and 127–160 ppm Ge. Interestingly, no Ge was detected in melilite by EPMA (detection limit was 90 ppm Ge) and LA-ICP-MS results with values above 100 ppm Ge indicates that some Ge-bearing glass inclusions might have been analysed together with the melilite matrix.

Some Ge was detected in olivine-group phases in the massive slags (olivine and monticellite; 140–150 ppm Ge), but glass is the principal host for Ge, especially in the granulated samples, which are richer in this element compared to massive slags (Tables 1, 3 and 4). Germanium concentrations in glass as detected by the EPMA range from <90 to 470 ppm (Table 4; Fig. 4). The LA-ICP-MS analyses of the glass matrices in the granulated slags indicated that the Ga and Ge concentration ranges are 98–182 ppm and 113–394 ppm, respectively (Table 5). However, many of the glass analyses obtained by LA-ICP-MS probably corresponded to mixtures with other phases because the glass phase contains submicrometric spinel dendrites and the laser spots were significantly larger (Supplementary Fig. S2).

Discussion

The phase assemblages and phase proportions in slags depend on the melt compositions, and melting and cooling conditions

Downloaded from http://pubs.geoscienceworld.org/minmag/article-pdf/85/6/879/5512245/s0026461x21000839a.pdf
by guest

Table 2. Selected electron microprobe analyses of spinels.

Sample	T17-1A	T17-1A	T17-1A	T17-1A	T17-1A	T17-1B	T17-1B	T18-1	T18-1	T17-2	T17-2
Spot no.	3	7	9	17	23	33	45	52	54	64	68
wt.%											
SiO_2	0.53	0.36	0.26	0.33	0.06	0.24	0.82	0.25	0.16	0.79	0.12
TiO_2	1.84	2.47	1.88	0.36	0.46	1.50	1.45	0.47	1.14	0.78	0.45
Al_2O_3	17.14	18.67	20.51	39.73	15.04	25.25	21.69	14.69	16.18	31.86	13.56
Cr_2O_3	0.86	–	0.50	3.17	48.59	0.09	1.80	28.35	6.45	15.56	42.09
Fe_2O_3*	42.19	41.11	40.97	17.33	6.60	35.54	36.17	22.30	40.45	12.21	9.49
FeO	17.05	16.78	15.50	9.01	15.49	15.47	16.13	11.33	13.94	8.58	9.30
MnO	0.31	0.34	0.29	0.17	0.28	0.24	0.27	0.19	0.16	0.13	0.24
MgO	3.48	4.07	4.74	6.55	11.70	4.74	4.32	6.04	5.19	6.98	7.53
CaO	0.45	0.22	0.24	0.55	0.28	0.48	0.76	0.25	0.66	0.94	0.16
K_2O	–	–	–	–	–	–	0.03	0.01	–	0.04	0.03
BaO	0.24	0.18	0.10	0.30	–	0.13	0.29	–	0.20	0.24	–
PbO	–	0.06	0.08	–	–		0.05		0.06	–	1.05
ZnO	13.48	13.93	14.24	19.44	0.59	13.95	13.35	14.25	12.33	18.21	13.06
CuO	0.04	–	–	0.05	0.04	–	–	–	0.03	0.07	0.31
CdO	–	–	–	–	–	0.03	–	–	–	–	–
Ga_2O_3	0.07	0.11	0.11	0.09	–	0.14	0.09	0.02	0.14	0.19	–
Total	97.66	98.30	99.42	97.08	99.13	97.80	97.21	98.15	97.09	96.57	97.38
Ga (ppm)	480	840	790	680	–	1060	670	170	1000	1370	–
Atoms per formula unit on the basis of 4 oxygens											
Si	0.019	0.013	0.009	0.010	0.002	0.008	0.028	0.008	0.005	0.026	0.004
Ti	0.049	0.065	0.048	0.009	0.011	0.038	0.038	0.012	0.030	0.019	0.012
Al	0.715	0.766	0.822	1.472	0.572	1.002	0.881	0.600	0.672	1.214	0.557
Cr	0.022	0.000	0.013	0.082	1.263	0.002	0.047	0.737	0.168	0.404	1.094
Ga	0.001	0.003	0.002	0.002	0.000	0.003	0.002	0.001	0.003	0.004	0.000
Fe^{3+}	1.124	1.077	1.049	0.410	0.160	0.901	0.938	0.582	1.073	0.297	0.249
Fe^{2+}	0.505	0.489	0.441	0.237	0.418	0.436	0.465	0.328	0.411	0.232	0.271
Mn	0.009	0.010	0.008	0.005	0.008	0.007	0.008	0.006	0.005	0.004	0.007
Mg	0.184	0.211	0.240	0.307	0.563	0.238	0.222	0.312	0.273	0.336	0.391
Ca	0.017	0.008	0.009	0.018	0.010	0.017	0.028	0.009	0.025	0.032	0.006
Zn	0.352	0.358	0.358	0.451	0.014	0.347	0.340	0.365	0.321	0.435	0.336
Cu	0.001	0.000	0.000	0.001	0.001	0.000	0.000	0.000	0.001	0.002	0.008
Species**	Mag	Mag	Mag	Ghn	Mchr	Hc	Mag	Zchr	Mag	Ghn	Mchr

*Fe_2O_3/FeO were calculated using the *End-Members Generator* (EMG, version 8.0) software by Ferracutti *et al.* (2015).
** Species identification according to spinel supergroup nomenclature and classification (Bosi *et al.*, 2019). Abbreviations: Hc – hercynite ($FeAl_2O_4$), Ghn – gahnite ($ZnAl_2O_4$), Mag – magnetite ($Fe^{2+}Fe^{3+}_2O_4$), Mchr – magnesiochromite ($MgCr_2O_4$), Zchr – zincochromite ($ZnCr_2O_4$).

(Piatak *et al.*, 2021). The position of bulk slag compositions and glass analyses in the ternary SiO_2–CaO–FeO diagram (Supplementary Fig. S3) indicates that the melting temperatures ranged from 1150 to 1400°C, similarly to other non-ferrous smelting slags (Vítková *et al.*, 2010; Warchulski *et al.*, 2015; Piatak *et al.*, 2021). The mineralogical compositions of the studied Ga- and Ge-bearing slags with dominant glass, spinel-group phases, melilite and olivine are consistent with the descriptions of the old slags produced from smelting in reverberatory and blast furnaces that were in operation in Tsumeb until 1996 (Ettler *et al.*, 2009a,b; Jarošíková *et al.*, 2017). The orders of the phase formation are spinel > melilite > olivine > glass for massive slags and spinel > melilite > glass for granulated slags. This is consistent with observations from other polymetallic slags (Ettler *et al.*, 2001; Ettler *et al.*, 2009a,b; Jarošíková *et al.*, 2017). The occurrence of melilite in the mineral assemblages indicates that the slag melt was rich in Ca (Warchulski *et al.*, 2016; Piatak *et al.*, 2021). Interestingly, clinopyroxene [$Ca(Mg,Fe)Si_2O_6$], a typical phase observed in many Cu and Pb–Zn slags (Lottermoser, 2002; Vítková *et al.*, 2010; Kierczak and Pietranik, 2011; Warchulski *et al.*, 2015, 2016), was not observed in the studied samples. Clinopyroxene was only detected in some Cu smelting slags from Tsumeb produced by the Ausmelt/TSL [Top-Submerged Lance] furnaces operating in Tsumeb until present times (Jarošíková *et al.*, 2017; Lohmeier *et al.*, 2021). This fact and the chemical compositions showing the predominance of Pb over Cu (Table 1), indicate that the Ga- and Ge-slags studied correspond to materials issued from the processing of the Cu-depleted portion of the tennantite [$(Cu,Fe)_{12}As_4S_{13}$]-dominated Cu–Pb ores, being the major source of Ga and Ge, which were mined from levels 34 to 46 of the Tsumeb deposit (Frondel and Ito, 1957; Gebhard, 1999; Melcher, 2003). These valuable elements probably do not originate from the fuel because our unpublished analyses show that their concentrations in the hard coal used in the Tsumeb smelter in 2012 were relatively low: 22.6 ± 0.16 ppm Ga and 33.1 ± 0.29 ppm Ge.

The concentrations of Ga (135–156 ppm) and Ge (128–441 ppm) in the slags studied (Table 1) correspond well to values reported previously for some of the Tsumeb slags: 47–194 ppm Ga (average: 102 ppm, $N = 21$; Lohmeier *et al.*, 2021), 200 ppm Ga and 183 ppm Ge (Höll *et al.*, 2007), and 220–280 ppm Ga and 350–690 ppm Ge (average: 245 ppm Ga, 455 ppm Ge, $N = 4$; Chirkst *et al.*, 2008). Other similar slags from Lubumbashi in the Democratic Republic of Congo exhibit concentrations of 100 ppm and 250 ppm Ge on the margin and in the core of the slag dump, respectively (Melcher and Buchholz, 2012).

The results presented here indicate that Ga is hosted primarily in spinel-group phases. According to the spinel supergroup nomenclature and classifications (Bosi *et al.*, 2019), the general formula of the oxyspinel subgroup is $A^{2+}B^{3+}_2O_4$. It is probable that Ga occurs as Ga^{3+} and substitutes for other trivalent cations due to similar ionic radii (Ga^{3+}: 0.62 Å, Cr^{3+}: 0.62 Å, Fe^{3+}: 0.55 Å,

Downloaded from http://pubs.geoscienceworld.org/minmag/article-pdf/85/6/879/5512245/s0026461x21000839a.pdf
by guest

Table 3. Selected electron microprobe compositional data for melilite- and olivine-group phases.

Sample	T17-1A	T17-1B	T17-1B	T17-2	T18-2		T17-1A	T17-1A	T17-1A	T17-1B
Spot no.	6	35	38	60	71		5	11	21	50
Phase	Melilite	Melilite	Melilite	Melilite	Melilite		Olivine	Olivine	Monticellite	Monticellite
wt.%						wt.%				
SiO_2	39.44	39.30	40.15	40.88	40.11	SiO_2	32.19	33.69	34.95	33.74
Al_2O_3	3.22	0.82	2.09	1.71	1.35	Al_2O_3	0.07	0.09	0.03	0.14
FeO	4.20	2.53	4.33	3.17	2.41	Cr_2O_3	0.17	–	–	0.05
MnO	0.08	0.16	0.08	0.09	0.05	FeO	38.19	31.03	13.22	18.30
MgO	5.29	3.84	6.72	7.28	6.17	MnO	1.48	1.19	0.67	0.45
CaO	36.76	36.34	37.71	37.94	37.37	MgO	14.89	21.37	14.67	11.38
Na_2O	0.05	–	–	–	–	CaO	4.34	3.50	30.71	30.38
K_2O	0.14	0.06	0.09	0.08	0.04	K_2O	0.02	–	–	0.02
BaO	0.17	0.49	0.20	0.12	0.09	BaO	–	0.17	0.10	–
PbO	0.15	0.20	0.09	0.09	0.16	ZnO	8.41	7.48	4.91	4.77
ZnO	8.56	13.27	6.79	7.32	9.80	P_2O_5	0.21	0.14	–	0.17
CuO	0.05	–	–	–	–	Total	99.98	98.65	99.26	99.39
Total	98.10	97.02	98.24	98.68	97.55					
Ga (ppm)	–	–	–	90	–	Ge (ppm)	–	150	140	–
Atoms per formula unit on the basis of 7 oxygens						Atoms per formula unit on the basis of 4 oxygens				
Si	1.944	2.007	1.962	1.980	1.988	Si	0.983	0.993	0.999	0.989
Al^{IV}	0.056	0.000	0.038	0.020	0.012	Al	0.003	0.003	0.001	0.005
Al^{VI}	0.131	0.050	0.082	0.078	0.067	Cr	0.004	0.000	0.000	0.001
Fe	0.173	0.108	0.177	0.128	0.100	Fe	0.976	0.765	0.316	0.448
Mn	0.003	0.007	0.003	0.004	0.002	Mn	0.038	0.030	0.016	0.011
Mg	0.388	0.292	0.489	0.525	0.456	Mg	0.678	0.939	0.625	0.497
Ca	1.941	1.989	1.974	1.969	1.984	Ca	0.142	0.111	0.940	0.954
Na	0.005	0.000	0.000	0.000	0.000	K	0.001	0.000	0.000	0.001
K	0.009	0.004	0.006	0.005	0.002	Ba	0.000	0.002	0.001	0.000
Ba	0.003	0.010	0.004	0.002	0.002	Zn	0.190	0.163	0.103	0.103
Pb	0.002	0.003	0.001	0.001	0.002					
Zn	0.312	0.501	0.245	0.262	0.359	% end-members (mol. %)*				
Cu	0.002	0.000	0.000	0.000	0.000	Lrn	8	6	50	50
% end-members (mol. %)*						Fo	37	51	33	26
Hdy	31	50	25	26	36	Fa	53	41	17	23
Åk	39	29	49	53	46	Tep	2	2	1	1
FeÅk	18	12	18	13	10					
Gh	6	4	4	4	4					
Aåk	6	5	4	4	4					

'–' not detected; *abbreviations: Hdy – hardystonite ($Ca_2ZnSi_2O_7$); Åk – åkermanite ($Ca_2MgSi_2O_7$); FeÅk – 'ferroåkermanite' ($Ca_2FeSi_2O_7$); Gh – gehlenite ($Ca_2Al_2SiO_7$); Aåk – alumoåkermanite ($CaNaAlSi_2O_7$; large cations K, Pb and Ba were associated with this end-member); Lrn – larnite (Ca_2SiO_4); Fo – forsterite (Mg_2SiO_4); Fa – fayalite (Fe_2SiO_4); and Tep – tephroite (Mn_2SiO_4).

Table 4. Selected electron microprobe compositional data for glass.

Sample	T17-1A	T17-1B	T18-1	T17-2	T17-2	T18-2	T18-2	T18-2	T18-2	T18-2	T18-2	T18-2			
Spot no.	4	34	59	70	2	73	80	81	14	19	20	21	min	max	mean*
wt.%															
SiO_2	33.73	33.58	36.70	28.57	30.22	26.27	28.46	28.00	25.41	25.57	25.75	25.67	23.08	36.70	27.93
TiO_2	0.07	0.12	0.10	0.24	0.33	0.21	0.25	0.23	0.19	0.25	0.25	0.24	0.04	0.33	0.22
Al_2O_3	5.34	4.92	4.22	4.48	4.93	3.80	4.27	4.40	3.77	4.03	4.05	4.01	3.51	5.40	4.30
Cr_2O_3	0.42	–	–	0.05	0.05	–	0.04	–	–	–	–	0.05	–	0.42	0.10
FeO	17.72	26.90	7.59	22.14	19.55	20.36	19.09	20.76	21.41	22.65	23.19	23.04	7.59	30.53	22.13
MnO	0.50	1.04	0.10	0.39	0.32	0.26	0.21	0.26	0.24	0.29	0.29	0.25	0.10	1.04	0.33
MgO	0.25	3.12	4.05	5.00	6.41	5.00	4.89	4.81	5.10	4.99	5.02	4.90	0.25	6.44	4.53
CaO	10.69	12.11	34.65	21.61	21.94	21.75	23.22	22.67	21.31	21.96	21.99	22.10	10.69	34.65	21.53
Na_2O	1.69	0.53	–	–	–	–	0.30	0.16	–	–	–	–	–	1.69	0.46
K_2O	5.16	1.93	0.23	0.52	0.75	0.55	0.59	0.64	0.54	0.53	0.58	0.56	0.23	5.16	0.78
BaO	4.50	2.09	0.26	0.58	0.57	0.36	0.54	0.48	0.37	0.14	0.40	0.30	0.14	4.50	0.65
PbO	0.78	0.79	0.23	1.42	0.86	0.85	1.50	1.21	0.96	1.47	1.65	1.40	0.23	2.84	1.39
ZnO	10.14	7.41	9.12	10.74	9.93	14.37	12.51	12.74	14.66	13.40	13.28	13.09	7.41	14.99	11.65
CuO	–	0.11	–	0.11	0.24	0.12	0.28	0.09	0.23	0.17	0.27	0.28	–	0.35	0.21
CdO	–	–	–	0.04	–	–	–	–	–	–	–	–	–	0.06	0.04
P_2O_5	2.25	1.17	0.34	0.16	0.12	0.20	0.29	0.26	0.17	0.26	0.20	0.24	0.08	2.25	0.33
SO_3	1.54	1.26	0.05	1.38	1.11	1.16	0.92	0.84	1.52	1.03	1.06	0.99	0.05	1.85	1.14
GeO_2	–	–	0.014	–	0.043	0.025	0.028	0.024	0.067	0.029	–	0.041	–	0.067	0.035
Total	94.79	97.07	97.63	97.43	97.36	95.29	97.40	97.59	95.93	96.80	98.03	97.15	94.79	99.27	97.29
Ge (ppm)	–	–	90	–	300	170	190	160	470	200	–	290		470	240

'–' not detected; *mean calculated for $N = 40$ analyses, except for CuO ($N = 37$), GeO_2 and Ge ($N = 16$), Na_2O ($N = 13$), Cr_2O_3 ($N = 12$) and CdO ($N = 4$).

Downloaded from http://pubs.geoscienceworld.org/minmag/article-pdf/85/6/879/5512245/s0026461x21000839a.pdf
by guest

Table 5. LA-ICP-MS data for Ga and Ge concentrations in individual phases (mean values or ranges of means).

Sample	Phase	*N*	Ga (ppm)	Ge (ppm)
T17-2	Glass matrix	12	127–176	113–269
T17-2	Melilite	6	74	127
T17-2	Spinel and glass mixture	4	99	23
T18-2	Glass matrix	26	98–182	340–394
T18-2	Glass with spinel dendrites	6	153	371
T18-2	Melilite	6	51	160
T18-2	Cr-spinel	5	36	5
T18-2	Spinel and glass mixture	6	33	73

Al^{3+}: 0.54 Å in octahedral coordination; Shannon, 1976). However, it is bound primarily in Zn–Fe–Al spinels (up to 1370 ppm Ga) (Table 2, Fig. 3). Interestingly, Ga was not substantially bound in Cr-bearing spinels (Table 2, Fig. 3). A recent study compared the Ga binding preferences in spinels from high-Al and high-Cr chromitites and found a similar phenomenon (Eliopoulos and Eliopoulos, 2019). Gallium concentrations were substantially higher in Al-rich spinels than in Cr-bearing spinels, because at magmatic conditions, Ga^{3+} shows a strong preference on tetrahedral sites where it can substitute for Al^{3+}, which can occupy both octahedral and tetrahedral sites in contrast to Cr^{3+}, which only occupies octahedral sites in the spinel structure (Eliopoulos and Eliopoulos, 2019). There is quite limited information about Ga content in phases produced from pyrometallurgy in the available literature. Avarmaa *et al.* (2018) studied Ga distribution during the secondary copper smelting and found, in agreement with our results, that Ga dissolves 3–4 times more in the spinel phase than in the silicate slag. Natural slags formed by fusion and recrystallisation during the burning of coal seams described by Kruszewski (2018) represent another analogy. Interestingly, Ga was not substantially partitioned into spinel phases in these materials; only one microprobe analysis indicated 222 ppm Ga in magnesioferrite, $MgFe_2O_4$ (Kruszewski, 2018). Whereas our LA-ICP-MS results indicate that Ga contents in melilite are relatively low (<74 ppm) (Table 5), Kruszewski (2018) reported 98–572 ppm Ga melilite-group phases from slags originating from coal burning. Other Ga-bearing phases were also found in these peculiar materials: chlormayenite, $Ca_{12}Al_{14}O_{32}[\square_4Cl_2]$ (up to 3.17 wt.% Ga), srebrodolskite, $Ca_2Fe^{3+}_2O_5$ (up to 772 ppm Ga), anorthite, $CaAl_2Si_2O_8$ (up to 301 ppm Ga), hematite, Fe_2O_3 (up to 210 ppm Ga), indialite, $Mg_2Al_2Si_5O_{18}$ (up to 220 ppm Ga) and ye'elimite, $Ca_4Al_6(SO_4)O_{12}$ (up to 580 ppm Ga) (Kruszewski, 2018).

Germanium is found mainly in glass (up to 470 ppm), although some concentrations were also detected in olivine-group phases (EPMA) and melilite (LA-ICP-MS) (Tables 3–5). Saini-Eidukat *et al.* (2016) demonstrated using the X-ray absorption fine structure (XAFS) spectroscopy that Ge in Ge-bearing willemite (Zn_2SiO_4) is present as Ge^{4+}, is four-fold coordinated with oxygen and substitutes for Si^{4+} due to similarities with the ionic radius (Ge: 0.39 Å and Si: 0.26 Å according to Shannon, 1976). We assume that the same mechanism is responsible for Ge preferential binding in glass and silicates in the slag materials studied. Due to the known geochemical affinity of Ge towards Fe^{3+}, it can also be hosted in secondary phases such as Fe(III) oxides and hydroxides (goethite, FeOOH or hematite, Fe_2O_3) in many deposits (Melcher and Buchholz, 2014; Mondillo *et al.*, 2018a,b). However, our slag samples are relatively unweathered, and practically no secondary Fe(III) oxides and hydroxides have been identified. In slag originating from coal burning, Kruszewski (2018) reported a Ge-bearing cuspidine ($Ca_4Si_2O_7(F,OH)_2$; up to 941 ppm Ge), but nothing similar was observed in our samples. However, Kruszewski (2018) also mentions that some melilites from these slag-like materials can contain up to 275 ppm Ge, which is comparable to our results (cf. Table 5).

The results obtained have important implications for the potential hydrometallurgical recovery of Ga and Ge from slags. Given that Ga is mostly found in spinel crystals <10 μm and Ge is concentrated in the glass matrix, forming a major part of the granulated slags volumetrically, ultrafine milling is needed to liberate Ga- and Ge-hosting phases for interaction with the leaching solution. Chirkst *et al.* (2008), in their first attempt to recover Ge from Tsumeb slags, milled the materials to <70 μm, which seems to be insufficient for the parallel liberation of Ga-bearing spinels from the samples reported here. More experimental work is needed to understand the optimum conditions for comminution of the slags (cf. Ettler *et al.*, 2020 and references therein), extraction, and recovery of Ga and Ge from these materials.

Conclusions

Old metallurgical slags from Tsumeb, Namibia are particularly rich in Ga (135–156 ppm) and Ge (128–441 ppm). A combination of PXRD, FEG-SEM-EPMA and LA-ICP-MS indicated that Ga and Ge have a different deportment in the slag phases. Gallium was hosted predominantly in Zn–Fe–Al spinels forming euhedral crystals <10 μm in size, which are enclosed in the silicate matrix (concentrations up to 1370 ppm Ga). In contrast, Ge was bound mostly in the silicate glass and, to a lesser extent, in other silicates (melilite and olivine-group phases). Germanium concentrations in the glass, being the dominant phase in granulated slags, vary in the range of 113–470 ppm. The results indicate that ultrafine milling is needed to liberate Ga- and Ge-hosting phases before potential extraction and recovery of Ga and Ge from the slag material. In addition, the highly variable concentrations observed indicate strict grade control is needed to optimise Ga and Ge recovery.

Acknowledgements. This study was supported by the Czech Science Foundation project (GAČR 19-18513S) and received institutional funding from the Center for Geosphere Dynamics (UNCE/SCI/006). We thank numerous colleagues for their support in the laboratories: Věra Vonásková, Lenka Jílková and Petr Drahota (PXRD). Hans Nolte, Pierre Reinecke and Mbabuu Trust of Dundee Precious Metals Tsumeb (DPMT) are thanked for providing us the old slag samples from Tsumeb. The thorough reviews of the Associate Editor and two anonymous reviewers helped to improve the original version of the manuscript.

Supplementary material. To view supplementary material for this article, please visit https://doi.org/10.1180/mgm.2021.83

References

Avarmaa K., Yliaho S. and Taskinen P. (2018) Recoveries of rare elements Ga, Ge, In and Sn from waste electric and electronic equipment through secondary copper smelting. *Waste Management*, **71**, 400–410.

Avarmaa K., Klemettinen L., O'Brien H., Taskinen P. and Jokilaakso A. (2019) Critical metals Ga, Ge and In: Experimental evidence for smelter recovery improvements. *Minerals*, **9**, 367.

Biver M. and Filella M. (2018) Germanium and solid sample digestion with aqua regia: the nescience of chemistry basic and its sequels. *Monatshefte für Chemie*, **149**, 461–465.

Downloaded from http://pubs.geoscienceworld.org/minmag/article-pdf/85/6/879/5512245/s0026461x21000839a.pdf
by guest

Bosi F., Biagioni C. and Pasero M. (2019) Nomenclature and classification of the spinel supergroup. *European Journal of Mineralogy*, **31**, 183–192.

Butcher T. and Brown T. (2014) Gallium. Pp. 150–176 in: *Critical Metals Handbook* (G. Gunn, editor). John Wiley & Sons, Hoboken, New Jersey, USA.

Chirkst D.E., Chistyakov A.A. and Cheremisina O.V. (2008) The hydrometallurgical method of obtaining of pure zinc and germanium oxides from the slag of copper-lead production. *Russian Journal of Non-Ferrous Metals*, **49**, 356–362.

Dey M., Hutton-Ashkenny M., Grogan J., Bowell R.J., Guilders R., Chueng L., Williams K.P., Evans T. and Goldsack D. (2010) The Minex Process: a novel process for the recovery of zinc and associated metals from metallurgical wastes. *Processing of Zinc Ores and Concentrates* '10. MEI, Cape Town, November 2010.

Drzazga M., Prajsnar R., Chmielarz A., Benke G., Leszczyńska-Sejda K., Ciszewski M., Bilewska K. and Krawiec G. (2018) Germanium and indium recovery from zinc metallurgy by-products – Dross leaching in sulphuric and oxalic acids. *Metals*, **8**, 1041.

Eliopoulos I.P.D. and Eliopolous G.D. (2019) Factors controlling the gallium preference in high-Al chromitites. *Minerals*, **9**, 623.

Ettler V., Legendre O., Bodénan F. and Touray J.C. (2001) Primary phases and natural weathering of old lead-zinc pyrometallurgical slag from Příbram, Czech Republic. *The Canadian Mineralogist*, **39**, 873–888.

Ettler V., Johan Z., Kříbek B., Šebek O. and Mihaljevič M. (2009a) Mineralogy and environmental stability of slags from the Tsumeb smelter, Namibia. *Applied Geochemistry*, **24**, 1–15.

Ettler V., Johan Z., Kříbek B. and Nolte H. (2009b): Mineralogy of primary phases in slags and matte from the Tsumeb smelter (Namibia). *Communications of the Geological Survey of Namibia*, **14**, 3–14.

Ettler V., Jarošíková A., Mihaljevič M., Kříbek B., Nyambe I., Kamona F. and Mapani B. (2020) Vanadium in slags from smelting of African Pb-Zn vanadate ores: Mineralogy, extractability and potential recovery. *Journal of Geochemical Exploration*, **218**, 106631.

European Commission (2020) *Study on the EU's list of Critical Raw Materials*. European Commission, Brussels, 157 pp.

Fayram T.S. and Anderson C.G. (2008) The development and implementation of industrial hydrometallurgical gallium and germanium recovery. *Journal of the Southern African Institute of Mining and Metallurgy*, **108**, 261–271.

Ferracutti G.R., Gargiulo N.F., Ganuza M.L., Bjerg E.A. and Castro S.M. (2015) Determination of the spinel group end-members based on electron microprobe analyses. *Mineralogy and Petrology*, **109**, 153–160.

Fortier S.M., Nassar N.T., Lederer G.W., Brainard J., Gambogi J. and McCullough E.A. (2018) *Draft critical mineral list – Summary of methodology and background information – U.S. Geological Survey technical input document in response to Secretarial Order No.* 3359. U.S. Geological Survey Open-File Report 2018–1021, 15 pp., https://doi.org/10.3133/ofr20181021.

Frenzel M., Ketris M.P. and Gutzmer J. (2014) On the geological availability of germanium. *Mineralium Deposita*, **49**, 471–486.

Frenzel M., Hirsch T. and Gutzmer J. (2016) Gallium, germanium, indium, and other trace and minor elements in sphalerite as a function of deposit type – A meta-analysis. *Ore Geology Reviews*, **76**, 52–78.

Frondel C. and Ito J. (1957) Geochemistry of germanium in the oxidized zone of the Tsumeb mine, South-West Africa. *American Mineralogist*, **42**, 743–753.

Gebhard G. (1999) *Tsumeb: A Unique Mineral Locality*. GG Publishing, Grossenseifen, Germany.

Gražulis S., Daškevič A., Merkys A., Chateigner D., Lutterotti L., Quirós M., Serebryanaya N.R., Moeck P., Downs R.T. and Le Bail A. (2012) Crystallography Open Database (COD): an open-access collection of crystal structures and platform for world-wide collaboration. *Nucleic Acids Research*, **40**, D420–D427.

Hofstra A., Lisitsin V., Corriveau L., Paradis S., Peter J., Lauzière K., Lawley C., Gadd M., Pilote J., Honsberger I., Bastrakov E., Champion D., Czarnota K., Doublier M., Huston D., Raymond O., VanDerWielen S., Emsbo P., Granitto M. and Kreiner D. (2021) *Deposit classification scheme for the Critical Minerals Mapping Initiative Global Geochemical Database*. U.S. Geological Survey Open-File Report 2021–1049, 60 pp., https://doi.org/10.3133/ofr20211049.

Höll R., Kling M. and Schroll E. (2007) Metallogenesis of germanium – A review. *Ore Geology Reviews*, **30**, 145–180.

Jarošíková A., Ettler V., Mihaljevič M., Kříbek B. and Mapani B. (2017) The pH-dependent leaching behavior of slags from various stages of a copper smelting process: Environmental implications. *Journal of Environmental Management*, **187**, 178–186.

Johan Z. (1988) Indium and germanium in the structure of sphalerite: an example of coupled substitution with copper. *Mineralogy and Petrology*, **39**, 211–229.

Kamona A.F. and Günzel A. (2007) Stratigraphy and base metal mineralization in the Otavi Mountain Land, Northern Namibia – a review and regional interpretation. *Gondwana Research*, **11**, 396–413.

Kierczak J. and Pietranik A. (2011) Mineralogy and composition of historical Cu slags from the Rudawy Janowickie Mountains, southwestern Poland. *The Canadian Mineralogist*, **49**, 1281–1296.

Kruszewski Ł. (2018) Geochemical Behaviour of Trace Elements in the Upper and Lower Silesian Basin Coal-Fire Gob Piles of Poland Pp. 407–449 in: *Coal and Peat Fires: A Global Perspective, vol. 5 – Case Studies – Advances in Field and Laboratory Research* (Stracher G.B., editor). Elsevier, Amsterdam, the Netherlands.

Liu F., Liu Z., Li Y., Liu Z., Li Q. and Li Z. (2016) Extraction of gallium and germanium from zinc refinery residues by pressure acid leaching. *Hydrometallurgy*, **164**, 313–320.

Lohmeier S., Lottermoser B.G., Schirmer T. and Gallhofer D. (2021) Copper slag as a potential source of critical elements – A case study from Tsumeb, Namibia. The *Journal of the Southern African Institute of Mining and Metallurgy*, **121**, 129–142.

Lottermoser B.G. (2002) Mobilization of heavy metals from historical smelting slag dumps, north Queensland, Australia. *Mineralogical Magazine*, **66**, 475–490.

Melcher F. (2003) The Otavi Mountain Land in Namibia: Tsumeb, germanium and Snowball Earth. *Mitteilungen der Österreichischen Mineralogischen Gesellschaft*, **148**, 413–435.

Melcher F. and Buchholz P. (2012) *Current and Future Germanium Availability from Primary Sources*. Minor Metals Conference, Cologne, 24 April 2012 [https://www.bgr.bund.de/DERA/DE/Downloads/vortrag_germanium.pdf].

Melcher F. and Buchholz P. (2014) Germanium. Pp. 177–203 in: *Critical Metals Handbook* (G. Gunn, editor). John Wiley & Sons, Hoboken, New Jersey, USA.

Melcher F., Oberthur T. and Rammlmair D. (2006) Geochemical and mineralogical distribution of germanium in the Khusib Springs Cu-Zn-Pb-Ag sulfide deposit, Otavi Mountain Land, Namibia. *Ore Geology Reviews*, **28**, 32–56.

Mondillo N., Herrington R., Boyce A.J., Wilkinson C., Santoro L. and Rumsey M. (2008a) Critical elements in non-sulfide Zn deposits: a reanalysis of the Kabwe Zn-Pb ores (central Zambia). *Mineralogical Magazine*, **82**, S89–S114.

Mondillo N., Arfè G., Herrington R., Boni M., Wilkinson C. and Mormone A. (2008b) Germanium enrichment in supergene settings: evidence from the Cristal nonsulfide Zn prospect, Bongará district, northern Peru. *Mineralium Deposita*, **53**, 155–169.

Moskalyk R.R. (2003) Gallium: the backbone of the electronic industry. *Minerals Engineering*, **16**, 921–929.

Moskalyk R.R. (2004) Review of germanium processing worldwide. *Minerals Engineering*, **17**, 393–402.

Piatak N.M. and Ettler V. (2021) Introduction: Metallurgical Slags – Environmental Liability or Valuable Resource? Pp.1–13 in: *Metallurgical Slags: Environmental Geochemistry and Resource Potential* (Piatak N.M. and Ettler V., editors). The Royal Society of Chemistry, Cambridge, UK.

Piatak N.M., Ettler V. and Hoppe D. (2021) Geochemistry and Mineralogy of Slags Pp. 59–124. in: *Metallurgical Slags: Environmental Geochemistry and Resource Potential* (Piatak N.M. and Ettler V., editors). The Royal Society of Chemistry, Cambridge, UK.

Saini-Eidukat B., Melcher F. and Lodziak J. (2009) Zinc-germanium ores of the Tres Marias Mine, Chihuahua, Mexico. *Mineralium Deposita*, **44**, 363–370.

Saini-Eidukat B., Melcher F., Göttlicher J. and Steininger R. (2016) Chemical environment of unusually Ge- and Pb-rich willemite, Tres Marias Mine, Mexico. *Minerals*, **6**, 20.

Downloaded from http://pubs.geoscienceworld.org/minmag/article-pdf/85/6/879/5512245/s0026461x21000839a.pdf
by guest

Shannon R.D. (1976) Revised effective ionic radii and systematic studies of interatomic distances in halides and chalcogenides. *Acta Crystallographica*, **A32**, 751–767.

Strnad L., Mihaljevič M. and Šebek O. (2005) Laser ablation and solution ICP-MS determination of rare earth elements in USGS BIR-1G, BHVO-2G and BCR-2G glass reference materials. *Geostandards and Geoanalytical Research*, **29**, 303–314.

Strnad L., Ettler V., Mihaljevič M., Hladil J. and Chrastný V. (2009) Determination of trace elements in calcite using solution and laser ablation ICP-MS: Calibration to NIST SRM glass and USGS MACS carbonate and application to real landfill calcite. *Geostandards and Geoanalytical Research*, **33**, 347–355.

USGS (2021a) *Gallium Data Sheet*. Mineral Commodity Summaries 2021, https://pubs.usgs.gov/periodicals/mcs2021/mcs2021-gallium.pdf

USGS (2021b) *Germanium Data Sheet*. Mineral Commodity Summaries 2021, https://pubs.usgs.gov/periodicals/mcs2021/mcs2021-germanium.pdf

Vítková M., Ettler V., Johan Z., Kříbek B., Šebek O. and Mihaljevič M. (2010) Primary and secondary phases in copper-cobalt smelting slags from the Copperbelt province, Zambia. *Mineralogical Magazine*, **74**, 581–600.

Warchulski R., Gaweda A., Kadziolka-Gawel M. and Szopa K. (2015) Composition and element mobilization in pyrometallurgical slags from the Orzel Bialy smelting plant in the Bytom–Piekary Slaskie area, Poland. *Mineralogical Magazine*, **79**, 459–483.

Warchulski R., Gaweda A., Janeczek J. and Kadziolka-Gawel M. (2016) Mineralogy and origin of coarse-grained segregations in the pyrometallurgical Zn–Pb slags from Katowice-Welnowiec (Poland). *Mineralogy and Petrology*, **110**, 681–692.

Warr L.N. (2021) IMA-CNMNC approved mineral symbols. *Mineralogical Magazine*, **85**, 291–320.

Yan S. and Swinbourne D.R. (2003) Distribution of germanium under lead smelting conditions. *Transactions of the Institution of Mining and Metallurgy Section C – Mineral Processing and Extractive Metallurgy*, **112**, C75–C80.

Downloaded from http://pubs.geoscienceworld.org/minmag/article-pdf/85/6/879/5512245/s0026461x21000839a.pdf
by guest